RESEARCH ARTICLE

Check for updates

White light emission from co-doped La₂Hf₂O₇ nanoparticles with suppressed host → Eu³⁺ energy transfer *via* a U⁶⁺ co-dopant†

Santosh K. Gupta, [ID] *[a,b] Brindaban Modak, [ID] [b,c] Pampa Modak[b,d] and Yuanbing Mao [ID] *[e]

Controlled energy transfer has been found to be one of the most effective ways of designing tunable and white photoluminescent phosphors. Utilizing host emission to achieve the same would lead to a new dimension in the design strategy for novel luminescent materials in solid state lighting and display devices. In this work, we have achieved controlled energy transfer by suppressing the host to dopant energy transfer in La₂Hf₂O₇:Eu³⁺ nanoparticles (NPs) by co-doping with uranium ions. Uranium acts as a barrier between the oxygen vacancies of the La₂Hf₂O₇ host and Eu³⁺ doping ions to increase their separation and reduce the non-radiative energy transfer between them. Density functional theory (DFT) calculations of defect formation energy showed that the Eu³⁺ dopant occupies the La³⁺ site and the uranium ion occupies the Hf⁴⁺ site. Co-doping the La₂Hf₂O₇:Eu³⁺ NPs with uranium ions creates negatively charged lanthanum and hafnium vacancies making the system highly electron rich. Formation of cation vacancies is expected to compensate the excess charge in the U and Eu co-doped La₂Hf₂O₇ NPs suppressing the formation of oxygen vacancies. This work shows how one can utilize the full color gamut in the La₂Hf₂O₇:Eu³⁺,U⁶⁺ NPs with blue, green and red emissions from the host, uranium and europium, respectively, to produce near perfect white light emission.

ᵃRadiochemistry Division, Bhabha Atomic Research Centre, Trombay, Mumbai 400085, India
ᵇHomi Bhabha National Institute, Anushaktinagar, Mumbai 400094, India. E-mail: santoshg@barc.gov.in, santufrnd@gmail.com; Tel: +91-22-25590636
ᶜChemistry Division, Bhabha Atomic Research Centre, Trombay, Mumbai 400085, India
ᵈRadiological Safety Division, Atomic Energy Regulatory Board, Anushaktinagar, Mumbai 400094, India
ᵉDepartment of Chemistry, Illinois Institute of Technology, 3101 South Dearborn Street, Chicago, IL 60616, USA. E-mail: ymao17@iit.edu; Tel: +1-312-567-3815
†Electronic supplementary information (ESI) available. See DOI: 10.1039/d1qi00134e

1. Introduction

Phosphor converted light emitting diodes (pc-LEDs) are considered one of the most extraordinary inventions in modern day owing to their extremely beneficial properties such low power consumption, high energy output, high brightness, environmental friendliness, *etc.*[1,2] To generate white light, some methods require mixing of red, green and blue light emitting phosphors or suitable dopant ions in a single host.[3,4] La₂Hf₂O₇ (LHO) has all the desirable credentials as a photoluminescence (PL) host owing to its low defect density, moderate phonon energy, optimum band gap, high thermal and structural stability, high radiation tolerance and ability to accommodate a large concentration of dopant ions at both A and B sites.[3,5,6] There have been reports including ours wherein LHO doped with various lanthanide ions (Ce³⁺, Pr³⁺, Sm³⁺, Eu³⁺, Tb³⁺, Dy³⁺, *etc.*) has been explored for visible photoluminescence and radioluminescence.[3,6–15] In the above-mentioned literature, Pr³⁺/Eu³⁺ doping is used for generating red emission, Sm³⁺ for orange, Tb³⁺ for green, Pr³⁺, Ti⁴⁺ for persistent luminescence, and Dy³⁺ for yellow/blue, *etc*. These ions create certain strains in the host lattice and could induce severe structural distortions to hamper the color efficiency of white light phosphors.[16] The role of luminescent hosts is found to be the key for optically active ions in relaxing forbidden f–f transition of lanthanide ions.[17,18] For most phosphors, the intrinsic emission of hosts due to charge transfer or defects is lost as most of the photoluminescence (PL) in these materials is triggered by host to dopant energy transfer (HDET).[19–21] Matching of energy states between luminescent hosts and dopant ions plays an important role in harvesting the light emission zone of LEDs.[22–25] There is no report on restricting host-dopant energy transfer to utilize the emissions of hosts and dopant ions. Singh *et al.* reduced the energy transfer efficacy of vanadate (VO₄³⁻) to lanthanide ion of YVO₄:Ln³⁺ by phosphorus co-doping.[26] Being a p-block element and

having a much smaller size compared to the 4f-block lanthanide ion, phosphorus encapsulation in the YVO_4 lattice leads to an unstable, strained and distorted phosphor.[27,28] Chung *et al.* used a blocking unit such as 2-phenylpropan-2-yl to suppress the HDET in organic phosphors.[29] There is a report on judiciously controlling HDET of $VO_4^{3-} \rightarrow Eu^{3+}$ by optimizing the dopant concentration in $YVO_4:Eu^{3+}$.[30]
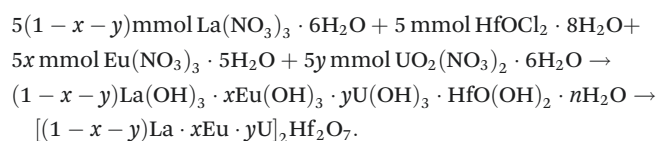
In general, when a lanthanide ion is selected as the co-dopant, it suffers from a poor absorption coefficient. On the other hand, the transition metal ion is unlikely to have a large overlap of the emission spectrum with the excitation spectrum of Eu. It was reported that uranium (UO_6^{6-}) and Eu^{3+} co-exist in the cubic lattice easily with the reported energy transfer of the 5f uranium ion to 4f Eu^{3+} in $ZnAl_2O_4$.[31] We are yet to find a report wherein defect emission is controlled by 5f ions to utilize the full electromagnetic spectrum.

Based on our recent studies on $A_2M_2O_7$ pyrochlore nanoparticles (NPs),[3,5,6] here we have co-doped 4f Eu^{3+} ions and 5f U^{6+} ions with a much closer size match inside the luminescent $La_2Hf_2O_7$ (LHO) host with controlled HDET. We judiciously utilized the emission of violet-blue (defect induced host emission), red (europium ion emission) and green PL (octahedral uranate emission) from LHO, LHO:Eu^{3+} (LHOE), and LHO:U^{6+} (LHOU) NPs, respectively, under UV irradiation to generate white light. Specifically, this work was undertaken to simultaneously utilize all three emission bands coming from the LHO host defect, europium and uranium to generate tunable emission and white color under single excitation wavelength while using Eu^{3+} as a dopant ion and U^{6+} as a co-dopant. Furthermore, theoretical modeling was carried out using density functional theory (DFT) to predict the local site of the dopant and the co-dopant and gain chemical insight into the role of the uranium dopant in quenching host to dopant energy transfer. This work offers a new strategy in the utilization of doped pyrochlore NPs for multicolor emission and a new way to inhibit HDET.

2. Experimental

The materials used in the synthesis are lanthanum nitrate hexahydrate $(La(NO_3)_3 \cdot 6H_2O, 99.0\%)$, hafnium dichloride oxide octahydrate $(HfOCl_2 \cdot 8H_2O, 98\%)$, europium(III) nitrate pentahydrate $(Eu(NO_3)_3 \cdot 5H_2O, 99.9\%)$, and uranyl nitrate hexahydrate $(UO_2(NO_3)_2 \cdot 6H_2O, 98–102\%)$. LHO, LHOE $(Eu^{3+} = 1.0\%)$, LHOU $(U^{6+} = 1.0\%)$, and LHOEU $(Eu^{3+} = 1.0\%$ and $U^{6+} = 0.1, 0.25, 0.5, 0.75, 1.0, 1.5,$ and $2.0\%)$ NPs were synthesized using a molten salt synthesis (MSS) method employing the $NaNO_3$–KNO_3 mixture as a molten salt at 650 °C.[5,6] The details of the synthesis process are well explained in the above-mentioned references. Specifically, stochiometric amounts of starting reactants were used with the LHOEU NPs as an example. First, $5(1 - x - y)$ mmol of $La(NO_3)_3 \cdot 6H_2O$, 5 mmol $HfOCl_2 \cdot 8H_2O$, $5x$ mmol $Eu(NO_3)_3 \cdot 5H_2O$, and $5y$ mmol $UO_2(NO_3)_2 \cdot 6H_2O$ were weighted and dissolved in 200 mL of de-ionized water (18.2 MΩ at 25 °C). The aqueous solution of the

starting reactants was mixed for 30 minutes using a magnetic stirring bar. Then, the solution was titrated with 200 mL of 10% ammonium hydroxide solution $(NH_4OH, 28–30\%)$ in a time range of 2 hours. A cloudy precipitate formed at the bottom of the beaker. The precipitate was collected through vacuum filtration, washed till the pH value of the filtrate solution was neutral, and then dried overnight in air at room temperature. This resulted in a final single-source complex precursor $(1 - x - y)La(OH)_3 \cdot xEu(OH)_3 \cdot yU(OH)_3 \cdot HfO(OH)_2 \cdot nH_2O$. In the second step, the LHOEU NPs were synthesized through a facile molten salt synthetic process using this single-source complex precursor and nitrate mixture $(NaNO_3 : KNO_3 = 1:1,$ molar ratio) at 650 °C for 6 hours. The empirical equations which govern the synthesis of the LHOEU NPs are:

$$5(1 - x - y)\text{mmol La}(NO_3)_3 \cdot 6H_2O + 5\text{ mmol HfOCl}_2 \cdot 8H_2O +$$
$$5x\text{ mmol Eu}(NO_3)_3 \cdot 5H_2O + 5y\text{ mmol UO}_2(NO_3)_2 \cdot 6H_2O \rightarrow$$
$$(1 - x - y)La(OH)_3 \cdot xEu(OH)_3 \cdot yU(OH)_3 \cdot HfO(OH)_2 \cdot nH_2O \rightarrow$$
$$[(1 - x - y)La \cdot xEu \cdot yU]_2Hf_2O_7.$$

Caution: ^{238}U (depleted uranium) is a weak α-emitting radionuclide with a half-life of 4.47×10^9 years. To avoid health risks, it should be handled carefully by trained personnel with all possible personal protective equipment (PPE) in a good quality lab equipped with a glove box and fume hood.

X-ray diffraction (XRD) was carried out using a BRUKER™ D8 X-ray Diffractometer with Cu $K_{\alpha1}$ radiation $(\lambda = 0.15406$ nm, 40 kV, 40 mA) by a 2θ scanning mode ranging from 10° to 90° and a scanning step size of 0.04° at a scanning rate of 2.0° min^{-1}. Raman spectra were elucidated using a Renishaw 2000 Micro-Raman spectrometer equipped with an argon laser (514.5 nm) in the range of 200–1000 cm^{-1}. The microstructure and morphology of the NPs were studied using a Carl Zeiss Sigma VP scanning electron microscope (SEM) equipped with a field emission gun operated at 5 kV. TEM images were recorded using a Hitachi HF 3300TEM/STEM. PL emission and excitation spectroscopy were investigated using an Edinburgh Instruments FLS980 fluorometer system equipped with a steady state xenon source.

The first-principles calculations were performed using a Vienna *ab initio* simulation package (VASP).[32,33] We performed the electronic structure calculations for $La_2Hf_2O_7$ in the presence and absence of dopant elements. The projector augmented wave (PAW) pseudo potentials were used for the ion-electron interactions including the valence states of La $(5p^65d^16s^2,$ 9 valence electrons), Hf $(5d^36s^1,$ 4 valence electrons), O $(2s^22p^4,$ 6 valence electrons), Eu $(5p^65d^16s^2,$ 9 valence electrons), and U $(5f^26s^26p^66d^27s^2,$ 14 valence electrons). The generalized gradient approximations (GGA) of Perdew–Burke–Ernzerhof (PBE) were used during the structure optimization procedure.[34,35] The plane wave basis with a kinetic energy cut off of 500 eV and an energy convergence of 10^{-6} eV for self-consistent iteration have been chosen. Brillouin zone sampling has been performed using a Γ-centered k-point mesh of $6 \times 6 \times 6$ using the Monkhorst and Pack scheme. For all the model structures, the relaxation of both cell parameters and ionic

This journal is © the Partner Organisations 2021

Inorg. Chem. Front., 2021, **8**, 3830–3842 | **3831**

positions during geometry optimization has been taken into account.[36] The calculation of density of states (DOS) were performed using a Γ-centered k-point mesh of $7 \times 7 \times 7$.

3.   Results and discussion

3.1.   X-ray diffraction (XRD)

Fig. 1a shows the XRD patterns of the LHO, LHOE (Eu^{3+} = 1.0%), LHOU (U^{6+} = 1.0%) and LHOEU (Eu^{3+} = 1.0% and U^{6+} = 1.0%) NPs. The XRD patterns show eight major identifiable diffraction peaks with (hkl) values of (222), (400), (440), (622), (444), (800), (662), and (840). They all are well in agreement with the reported XRD pattern of undoped and doped La$_2$Hf$_2$O$_7$.[3] It is clearly seen that neither U/Eu doping nor Eu and U co-doping distorted the basic La$_2$Hf$_2$O$_7$ pyrochlore structure. The calculated crystallite sizes using the Debye–Scherer equation and lattice parameter of the four above-mentioned samples are provided in Table 1. The calculated crystallite sizes are not affected much and are in the range of 27.4–28.8 nm for all the samples.

The lattice parameter did show some variations compared to that of the undoped LHO NPs (10.83 Å) with reduction for both LHOE (10.77 Å) and LHOU NPs (10.68 Å) whereas the LHOEU NPs assumed a value of 10.71 Å. This is expected due to the smaller ionic radius of both Eu^{3+} (1.07 Å) and U^{6+} (0.86 Å) compared to La^{3+} (1.16 Å) in 8-coordination.

However, it should be noted that XRD sometimes fails to sense the presence of weak pyrochlore reflections, which should be confirmed with further structural analysis by other techniques such as Raman spectroscopy.

3.2.   Raman spectroscopy

Radius ratio (r_A/r_B) plays an important role in deciding the exact structure of A$_2$B$_2$O$_7$ compounds. When $r_A/r_B > 1.46$, an

Table 1   Calculated crystallite sizes and lattice parameters of the LHO, LHOE, LHOU, and LHOEU NPs

NPs	Crystallite size (nm)	Lattice parameter (Å)
LHO	27.4 ± 0.5	10.83
LHOE	28.8 ± 0.5	10.77
LHOU	27.7 ± 0.5	10.68
LHOEU	28.7 ± 0.5	10.71

ordered pyrochlore of A$_2$B$_2$O$_7$ compounds is the most prevalent structure.[37] Based on the concepts of group theory, the Raman spectra of ideal pyrochlore A$_2$B$_2$O$_7$ compounds ($Fd\bar{3}m$ space group) consist of six well-defined sharp vibrational peaks in the range 200–1000 cm^{-1}, which are ascribed to A$_{1g}$ + E$_g$ + 4F$_{2g}$.[38,39] LHO prefers to stabilize in an ideal pyrochlore structure due to r_{La} (CN = 8) = 1.16 Å and r_{Hf} (CN = 6) = 0.710 Å giving a radius ratio value r_{La}/r_{Hf} = 1.63. Fig. 1b shows the Raman spectra of the LHO, LHOE, LHOU, and LHOEU NPs. All of them exhibited peaks located approximately at 306, 320, 397, 498, 519, and 615 cm^{-1} which correspond to F$_{2g}$, E$_g$, F$_{2g}$, A$_{1g}$, F$_{2g}$, and F$_{2g}$ modes, respectively.[40] Specifically, the peaks at 306, 320, and 397 cm^{-1} originate from the vibrations of the metal–oxygen bonds (in this case, La–O and Hf–O bonds, respectively). The peaks at 519 cm^{-1} and 615 cm^{-1} arise from the Hf–O stretching whereas the 498 cm^{-1} peak arising from the A$_{1g}$ mode is ascribed to the bending of the Hf–O bond in HfO$_6$ octahedra.[41] The small peak around 769 cm^{-1} is ascribed to the distortion of the HfO$_6$ octahedra.[42] Therefore, based on our Raman data, all four of these samples showed the ideal pyrochlore structure. Moreover, the 769 cm^{-1} peak intensified in the order of LHO, LHOU, LHOE, and LHOEU NPs, which suggested that doping of Eu^{3+} and U^{6+}, especially their co-doping, led to increased distortion of HfO$_6$ octahedra.
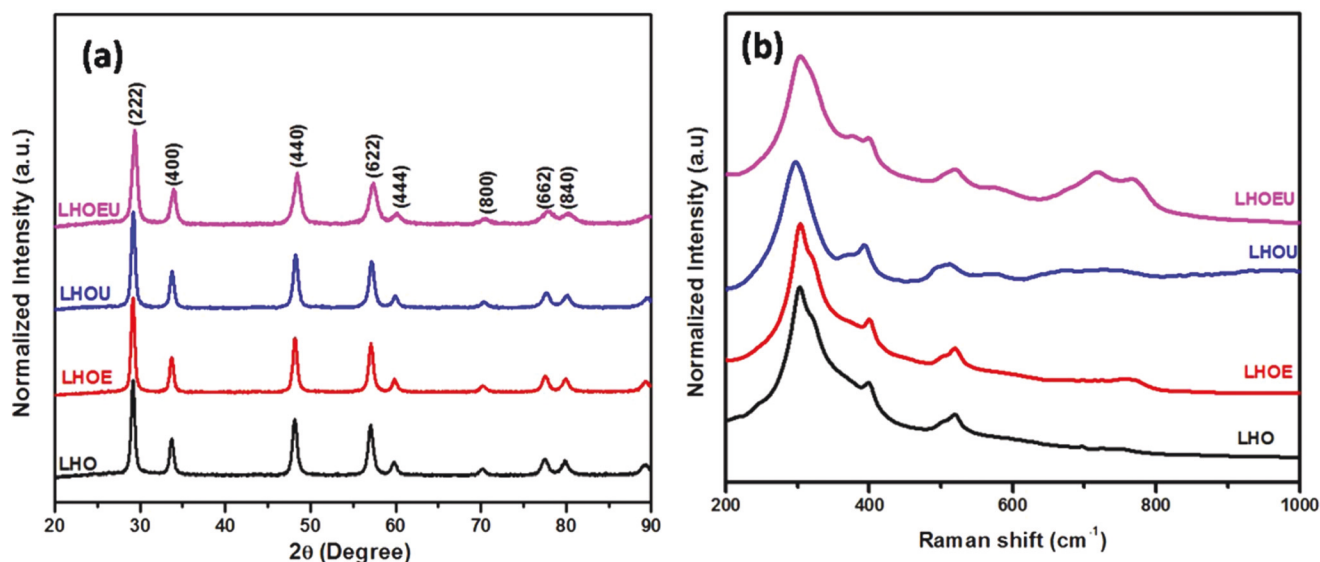

Fig. 1   (a) XRD patterns and (b) Raman spectra of the LHO, LHOE, LHOU, and LHOEU NPs.

3.3. Geometry and electronic structure of LHO

La$_2$Hf$_2$O$_7$ crystallizes in the cubic perovskite structure, in which La sits on the polyhedral LaO$_8$, coordinated to eight oxygen, and Hf sits on the polyhedral HfO$_6$, coordinated to six oxygen (Fig. 2a). Our calculated value of the equilibrium lattice parameters using the PBE functional is 10.83 Å (volume = 1270 Å^3) which is in good agreement with the experimental value of 10.776 Å.[43] Fig. 2b shows the calculated DOS and PDOS of pure La$_2$Hf$_2$O$_7$. It is evident that the valence band maxima (VBM) are mainly composed of O 2p states. The bottom part of the conduction band (CB) mainly originates from La 4f states with minor contribution of La 5d and Hf 5d states. Our calculated band gap is 4.30 eV, which is close to the earlier DFT calculated value of 4.18 eV,[9] but it is lower than the experimental value of 5.6 eV.[44]

3.4. Morphological study: SEM and TEM

Fig. 3a–d shows the SEM images of the LHO, LHOE, LHOU, and LHOEU NPs, respectively. The SEM micrographs show the formation of nanosized ellipsoids with an average diameter (corresponding size distribution histograms shown in Fig. S1†) in close agreement with the calculated crystallite size using the Debye–Scherer equation from the XRD data (Fig. 1a). All SEM images clearly showed that the as-synthesized particles are in the nanosized domain and spherical in shape. However, there is a certain degree of agglomeration in all these samples. The high surface area to volume ratio of NPs provides a very high surface energy. To minimize the surface energy, NPs tend to agglomerate, especially during the drying process after cast-dropping their dispersion on the SEM sample holder. Agglomeration of NPs may occur due to the attractive van der Waals forces between them. The morphology of these NPs remain the same with well-defined grain boundaries even with Eu or U doping and Eu,U co-doping into the LHO host

showing the capability of our synthesis procedure. Representative TEM images of the LHO and LHOU NPs (Fig. 3e and f, respectively) clearly show the formation of slightly agglomerated ellipsoidal NPs.

3.5. DFT calculated defect formation energies

In the present study, we have considered 88 atoms cell of the LHO host for the construction of the doped systems. For Eu doping, we have considered two scenarios, substitution of one La by Eu (Eu$_{La}$) and substitution of one Hf by Eu (Eu$_{Hf}$). Similarly, for U doping into La$_2$Hf$_2$O$_7$, we have considered two scenarios, substitution at the La lattice site (U$_{La}$) and substitution at the Hf lattice site (U$_{Hf}$). Similarly, for (Eu,U)-co-doped La$_2$Hf$_2$O$_7$, we have considered four different possibilities: (1) doping of both Eu and U at the La lattice sites (Eu$_{La}$ + U$_{La}$), (2) doping of both Eu and U at the Hf lattice sites (Eu$_{Hf}$ + U$_{Hf}$), (3) doping of Eu at the La lattice site while U at the Hf lattice site (Eu$_{La}$ + U$_{Hf}$), and (4) doping of Eu at the Hf lattice site while U at the La lattice site (U$_{La}$ + Eu$_{Hf}$). In each case, we have considered two different geometries by varying the relative distance between the two dopant elements. For the first case, we have chosen the nearest neighboring lattice sites while they are far away from each other for the second case. Comparison of the energy of the optimized geometries for the model structures indicates that both the structures are energetically very close to each other (energy difference range = 0.002–0.05 eV). To find out the preferred lattice site of the LHO host for Eu and U doping, the defect formation energies of different configurations have been computed using the below relation:[45,46]

$$\Delta H_f = E_{\text{defect}} - E_{\text{perfect}} + q \sum n_x \mu_x \qquad (1)$$

where E_{defect} and E_{perfect} represent the energy of the doped and perfect La$_2$Hf$_2$O$_7$ calculated with the same supercell size, μ_x

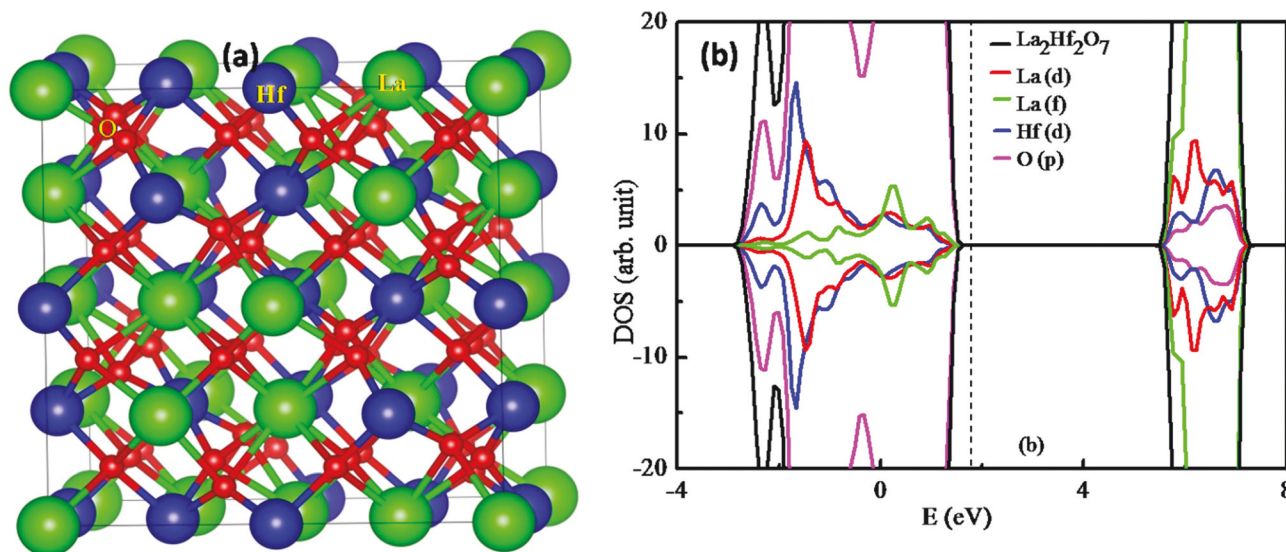**Fig. 2** Calculated (a) crystal structure and (b) density of states of La$_2$Hf$_2$O$_7$. Vertical dashed line in (b) indicates the Fermi level.
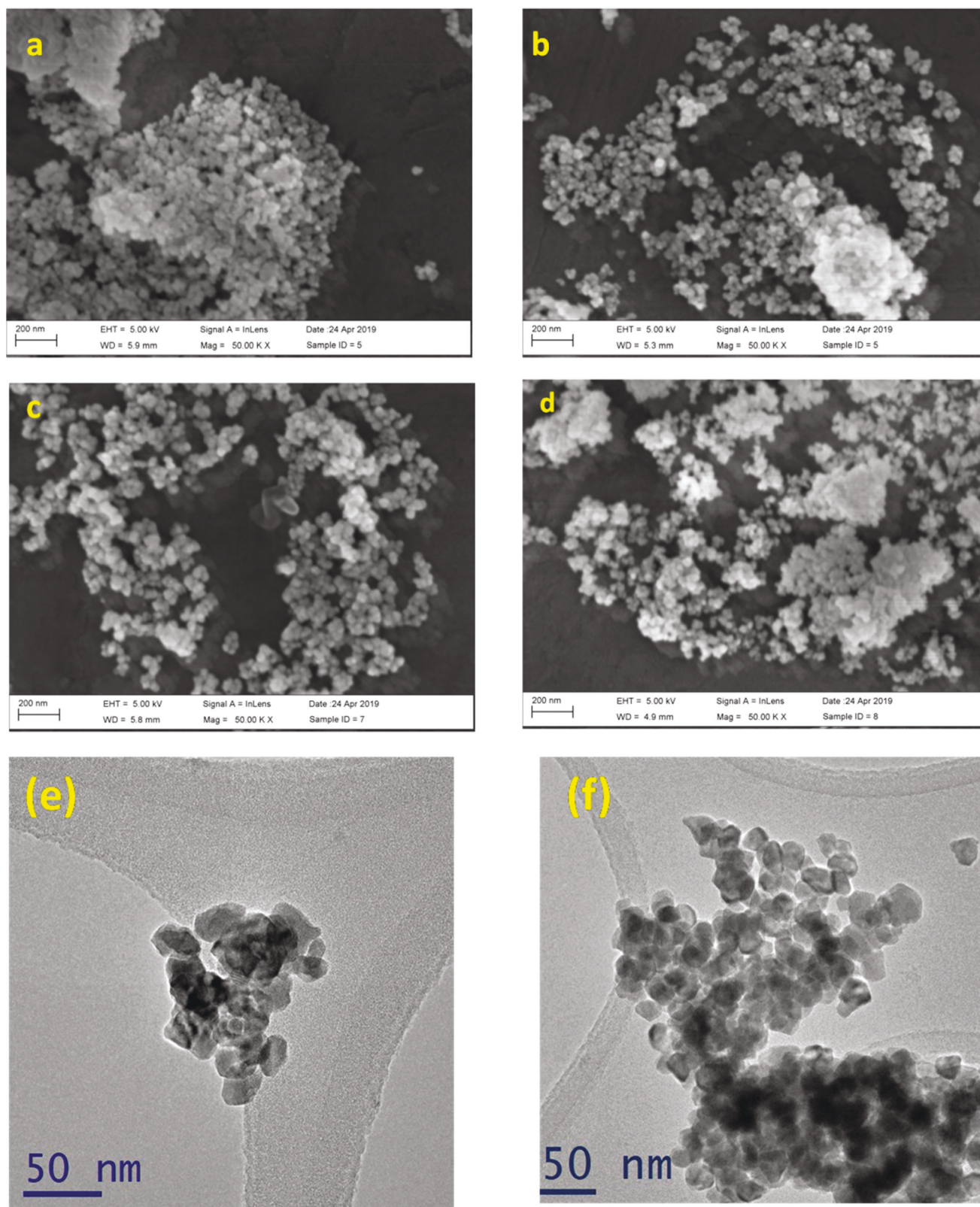
Fig. 3   SEM images of the (a) LHO, (b) LHOE, (c) LHOU, and (d) LHOEU NPs. Representative TEM images of the (e) LHO and (f) LHOU NPs.

indicates the chemical potential of the element X, and n_x is the number of elements added ($q = -1$) or replaced ($q = +1$) to form the defect system. The formation energy for doping of Eu at the La site is lower by 3.44 eV in comparison to that of Eu doping at the Hf site. This indicates preferential occupation of Eu atoms at the lanthanum (La^{3+}) site over the hafnium (Hf^{4+}) site. Therefore, the calculated defect formation energy of the Eu-doped $La_2Hf_2O_7$ system reveals that the probability of formation of the Eu_{La} defect is more favorable in comparison to that of Eu_{Hf}. In contrast to Eu, uranium shows higher preference to the Hf lattice site over the La site. The calculated formation energy for U_{Hf} is found to be lower by 0.56 eV with respect to that of U_{La}. On the other hand, for Eu and U co-doped $La_2Hf_2O_7$, the calculated defect formation energy follows the order (Eu_{La} + U_{Hf})-$La_2Hf_2O_7$ (0.82 eV) < (Eu_{Hf} + U_{Hf})-$La_2Hf_2O_7$ (0.90 eV) < (U_{La} + Eu_{Hf})-$La_2Hf_2O_7$ (1.45eV) < (Eu_{La} + U_{La})-$La_2Hf_2O_7$ (1.84eV). Thus, based on the formation energy calculation it can be concluded that the co-doping with Eu at the La lattice site and U at the Hf lattice site is energetically most favorable. This behavior is consistent with that of the individual doped systems.

3.6. PL

Fig. 4a shows the PL emission spectrum of LHO NPs under 305 nm. The emission spectra showed a broad band around 400 nm in the violet-blue region. We have used DFT calculations in our earlier work to probe the same and found that

the presence of doubly ionized oxygen vacancies (V_O^{2+}) is the most probable defect responsible for visible PL in LHO NPs.[6,9] The violet-blue emission in the LHO NPs is attributed to electronic transition from the defect state located around 3.5 eV to the valence band maxima (VBM). The recombination of photo-excited holes with electrons present in the OVs leads to violet blue emission in the LHO NPs. The excitation spectrum of the LHO NPs (λ_{em} = 400 nm) is shown in Fig. 5a which depicts a broad band peaking around 305 nm which was ascribed to the combined effect of electronic transitions involving defect states and $O^{2-} \rightarrow Hf^{4+}$ ion.

Fig. 4b shows the emission spectra of the LHOE NPs under 305 nm which displayed the typical Eu^{3+} features of $^5D_0 \rightarrow {}^7F_J$ (J = 1–4) transitions. The spectrum displayed an intense peak at 616 nm due to the hypersensitive electric dipole transition compared to the peak at 591 nm due to the magnetic dipole transition. This suggests low local symmetry around the europium ion in the LHO host which is in line with our earlier report on the LHOE NPs.[6,9] Fig. 5b shows the typical excitation spectra of the LHOE NPs consisting of a broad $O^{2-} \rightarrow Eu^{3+}$ charge transfer band in the region of 200–300 nm and fine intra-configuration f–f transition features of Eu^{3+} in the region of 350–550 nm.

Surface defects and cation vacancies are deleterious to PL as they provide non-radiative pathways and may quench the luminescence. However, oxygen vacancies lead to enhanced PL in the case of doped phosphors by acting as sensitizers and
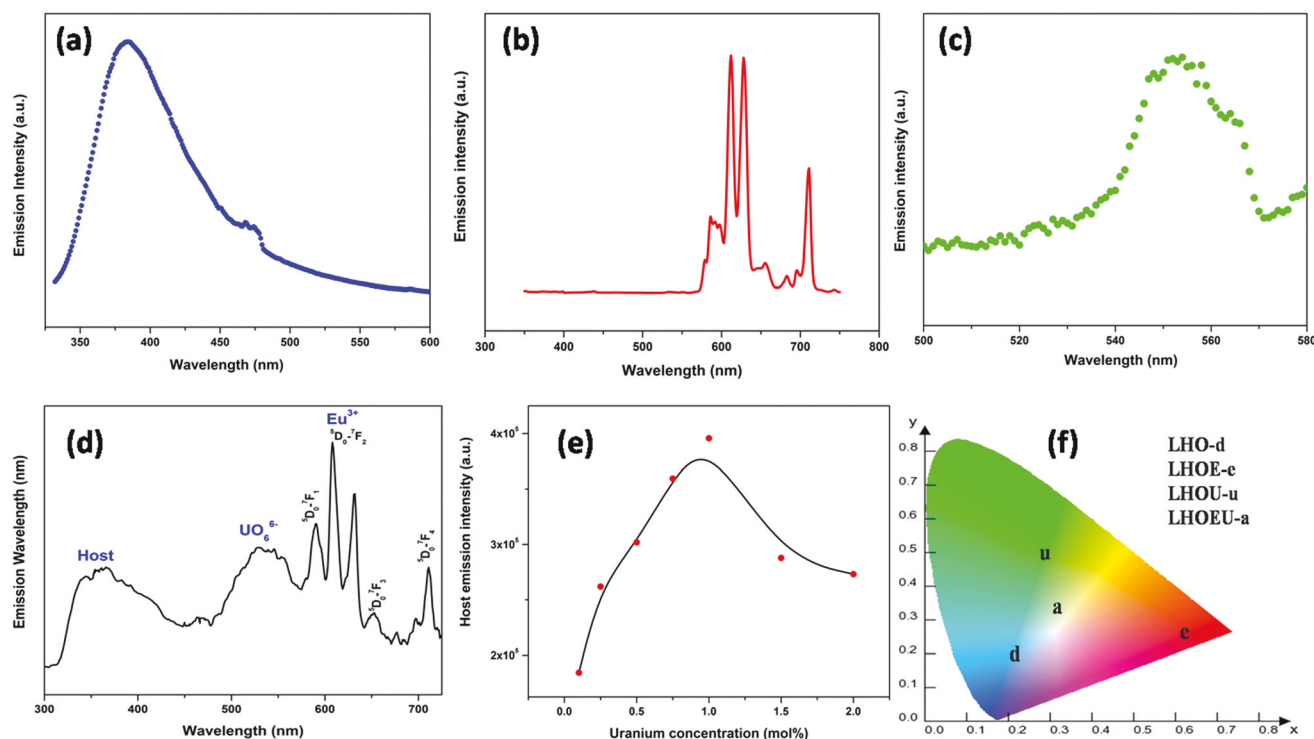

Fig. 4 Emission spectra of the (a) LHO, (b) LHOE, (c) LHOU, and (d) LHOEU NPs under 305 nm excitation. (e) Effect of uranium doping concentration on PL emission intensity of the LHO host co-doped with Eu^{3+} in the wavelength range of 300−450 nm. (f) Color coordinate diagram showing light emitted from the LHO, LHOE, LHOU, and LHOEU NPs.
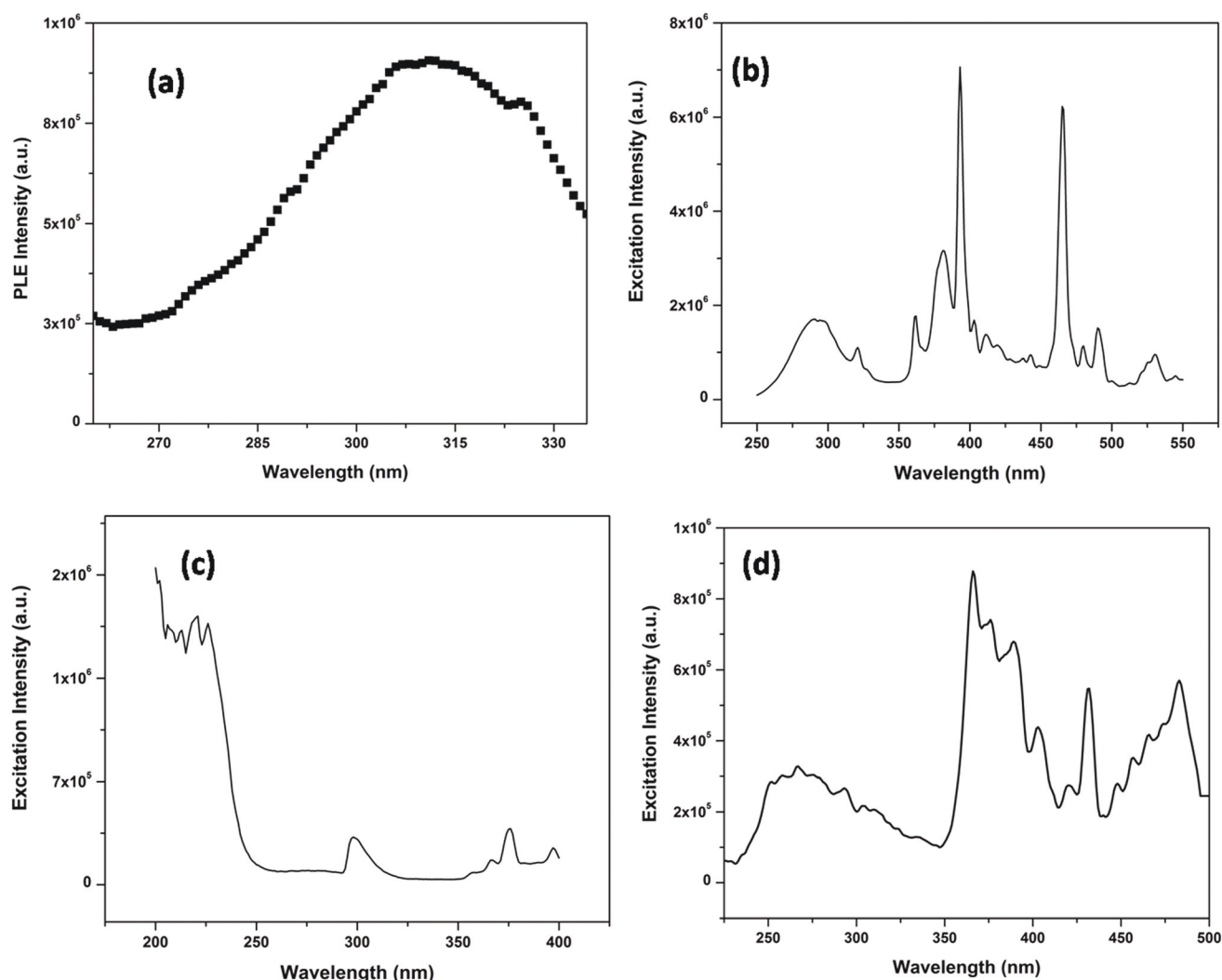
Fig. 5 Excitation spectra of the (a) LHO (λ_{em} = 400 nm), (b) LHOE (λ_{em} = 616 nm), (c) LHOU (λ_{em} = 556 nm), and (d) LHOEU (λ_{em} = 616 nm) NPs.

mediate HDET, and the process is known as host sensitized energy transfer (HSET).[47] A wide band gap of LHO (~4.3 eV) may easily accommodate Eu^{3+} 4f energy levels which lead to a strong interaction between the O^{2-} 2p states and Eu^{3+} d/f states enabling efficient HDET.[48] In the LHOE NPs, energy transfer is induced through doubly ionized oxygen vacancies (V_O^{2+}) lying in the LHO band gap to the Eu^{3+} excited levels. The Eu^{3+} d/f states are present in both VB and CB minority and majority spin components in the LHO host.[9] The HSET mechanism is shown schematically in Fig. S2.† Based on the Dexter concept of energy transfer, efficient energy transfer can only happen when there is a spectral overlap between the donor emission and the acceptor excitation (LHO and Eu^{3+} ion, respectively, in this case).[49] To further validate these results, our experimental results with clear spectral overlap between the emission of the LHO host (donor) and excitation of Eu^{3+} ion (acceptor) (Fig. 6a) suggested an efficient energy transfer from the host to the dopant ions. Fig. 6b clearly shows complete disappearance of host emission in the case of the LHOE

NPs when compared with the emission spectrum of the LHO NPs while both the emission spectra were recorded under the identical conditions of excitation wavelength, slit width, and dwell time to avoid any discrepancies.

Fig. 4c shows the emission spectra (λ_{ex} = 305 nm) of the LHOU NPs wherein a broad band peaking at 556 nm was observed which is typical of uranium in the +6 oxidation state existing in the form of octahedral uranate (UO$_6^{6-}$) having a U–O moiety.[5] It arises due to ligand to metal charge transfer (LMCT) involving bonding oxygen (Π_u, Π_g, Ω_g, and Ω_u orbitals) to nonbonding uranium (5f$_\delta$ and 5f$_\Phi$ orbitals). Fig. 5c shows the excitation spectra (λ_{em} = 556 nm) of the LHOU NPs which displayed dual features of a shoulder spanning 200–250 nm ascribed to the O^{2-} → U^{6+} charge transfer band and the fine features in the range of 300–400 nm because of the intra-configuration f–f bands of the uranium ion.

Fig. 4d shows the emission spectrum of the LHOEU NPs (1.0% Eu^{3+} and 1.0% U^{6+}) at 305 nm excitation. Here we found that the efficient HDET previously observed in the case of the
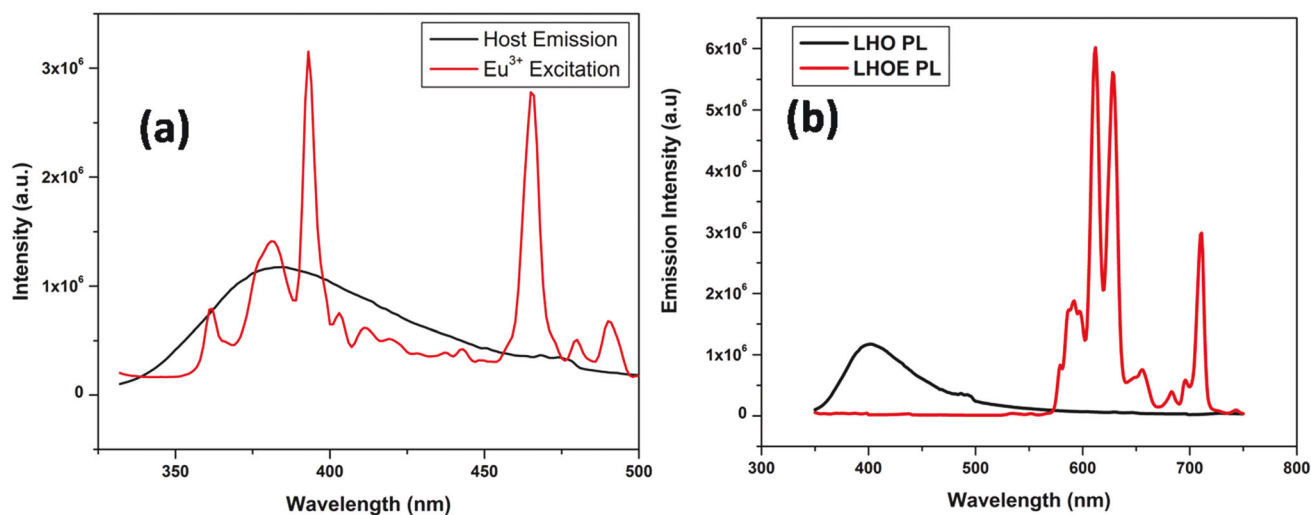
Fig. 6 (a) The emission spectrum of the LHO NPs and the excitation spectrum of the LHOE NPs and (b) PL emission spectra of the LHO and LHOE NPs showing the energy transfer from the LHO host to the Eu^{3+} ion in the LHOE NPs.

LHOE NPs was completely curtailed off. This emission spectrum was rich in all three components: defect induced blue emission, uranium induced green emission, and europium induced red emission. The efficacy of HDET was further confirmed by monitoring the PL emission of the LHOEU NPs with varying uranium doping concentrations from 0.1 to 2.0 mol% (Fig. 7a).

Uranium doping suppresses the formation of OVs but the europium PL can be seen from the LHOEU NPs. This is because the excitation at 305 nm can also directly excite the europium ion through its intra-configurational f–f contribution of the $^7F_0 \rightarrow {}^5H_6$ transition.[50] The proposed contrasting mechanisms of europium PL in the LHOE and LHOEU NPs are shown in Fig. S3.†

We have also calculated the color coordinates of the LHOEU NPs for different uranium concentrations (Fig. S4†). Clear color tunability from red to near white to white emission can be seen. The digital camera image of the LHOE and LHOEU NPs (Fig. S5†) clearly show red and white emissions from the respective samples.

XRD patterns showed no impurity or any phase separation from the LHOEU NPs at different uranium concentrations (Fig. 7b). All these LHOEU NPs were single phase samples matching with the LHO host having an $Fd\bar{3}m$ space group and an ordered pyrochlore structure.

It is clearly seen from Fig. 7a that the host emission increased as the uranium concentration increased up to 1.0 mol%, and then reduced beyond 1.0% uranium doping
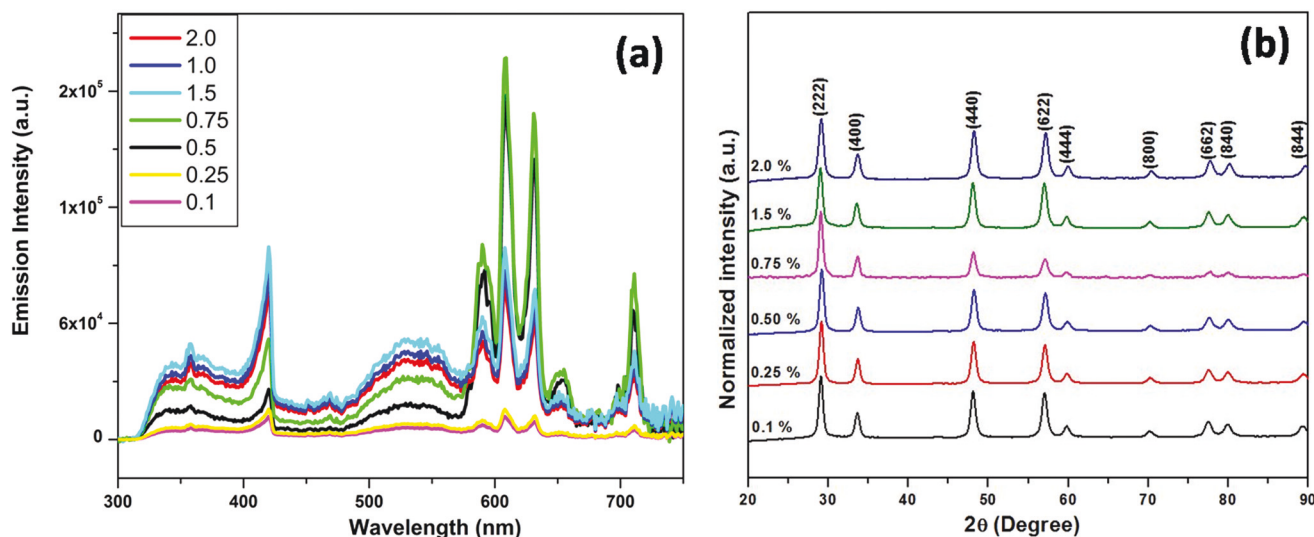

Fig. 7 (a) Emission spectra of the LHOEU NPs with different uranium doping concentrations (0.1–2.0 mol%) under 305 nm excitation and (b) XRD patterns of the LHOEU (%U = 0.1, 0.25, 0.5, 0.75, 1.5, and 2.0) NPs.

This journal is © the Partner Organisations 2021

Inorg. Chem. Front., 2021, **8**, 3830–3842 | **3837**

concentration owing to the reduced density of oxygen vacancies. DFT calculations of the most stable local site of uranium in the LHO host suggested that uranium has high probability to stabilize at the Hf^{4+} site compared to the La^{3+} site whereas the reverse is true for the europium ion. As more and more U^{6+} ion is co-doped inside the LHO lattice, there is a progressive increase in the density of hafnium vacancies and antisite defect (U@Hf) to induce the need for charge compensation owing to aliovalent substitution of the U^{6+} ion at the Hf^{4+} site. Presence of negatively charged cation vacancies may annihilate the positively charged oxygen vacancies intrinsically present in the pyrochlore structured LHO. This initial increase of the host emission with the increase of uranium concentration up to 1.0 mol% can be ascribed to the suppression of energy transfer from the LHO host to the europium ion. This suppression of HDET by uranium can be ascribed to different mechanisms. Firstly, uranium ion acted as a barrier between the LHO host and the dopant (Eu^{3+}) inside the LHOEU NPs to inhibit HDET. It is believed that co-doping uranium in the LHOE lattice enhanced the separation between the defect sites and the europium dopant which reduced the HDET and rather led to an increase in violet-blue emission due to an increased probability of radiative recombination of photoexcited holes and electrons in the valence band. The excitation spectrum of the LHOEU NPs (Fig. 5d) also clearly showed the typical features of defects, uranium and europium, which further suggested that uranium acts as a barrier to increase the separation between the defect and europium ion. In particular, several fine peaks in the region of 350–500 nm can be ascribed to the Eu^{3+} f–f transitions of $^7F_0 \rightarrow {}^5H_6$ (300 nm), $^7F_0 \rightarrow {}^5H_3$ (320 nm), $^7F_0 \rightarrow {}^5D_4$ (360 nm), $^7F_0 \rightarrow {}^5G_J$ (385 nm), $^7F_0 \rightarrow {}^5L_6$ (395 nm), $^7F_1 \rightarrow {}^5D_3$ (416 nm), and $^7F_0 \rightarrow {}^5D_2$ (464 nm).

Secondly, charge neutralization requires the occupancy of $3Hf^{4+}$ sites by $2U^{6+}$ ions leading to the formation of a cation vacancy V_{Hf}'''' and an antisite defect $U_{Hf}^{····}$. These defects absorb the photons emitted by the LHO host and back transfer to the host itself. This back transferred energy to the europium ion enhanced the LHO host emission itself. Phosphorus ion is also reported to minimize non-radiative energy transfer between the vanadate host and the Dy^{3+} ion.[26]

A color coordinated diagram of the LHO, LHOE, LHOU and LHOEU NPs is shown in Fig. 4f. The violet-blue (marked as letter d), red (marked as letter e), and green (marked as letter u) light emissions can be clearly seen from the LHO, LHOE, and LHOU NPs, respectively. The interesting part is that the color coordinates of the LHOEU NPs indicated the color domain close to 0.312 and 0.323 giving almost perfect white light (Fig. 4 f indicated by letter a). This is due to the combined emissions from the blue, green and red hues. The quantum yield (QY) of the LHOE NPs has been previously reported to be ~16.5%,[8] whereas the QY of the LHOEU NPs depicting white light emission calculated in this work was found to be approximately 12.4%. Compared to commercial white phosphors, it is low and further improvement is necessary. Considering the potential of tuning the color coordinates by actinide doping and the efficacy of LHO as a luminescence

host, we will explore several other strategies to improve the QY in our future work. These strategies could include quenching surface defects by a core–shell strategy, annealing out charge compensating defects, co-doping by alkali ions, and co-precipitating pH and optimizing the ideal thermal conditions in MSS. In our previous work on $La_2Hf_2O_7$:Eu^{3+} (ref. 9) and $La_2Hf_2O_7$:Sm^{3+},[7] we carried out *in situ* PL measurements and found that the activation energies for thermal quenching were 0.41 eV and 0.153 eV, respectively, highlighting the potential of LHO as a luminescent host. In particular, the thermal stability of the $La_2Hf_2O_7$:Eu^{3+} NPs was quite good with 54% intensity retained up to 700 K.

4. DFT calculations

4.1. Electronic structure of LHOE

To investigate the effect of Eu doping on the electronic structure of $La_2Hf_2O_7$, we have calculated DOS for both types of Eu defects, *i.e.*, substitution of one La or Hf site by a Eu ion (Eu_{La} and Eu_{Hf}, respectively). Fig. 8a and b show the DOS plots for $La_2Hf_2O_7$ with the Eu_{La} and Eu_{Hf} defects, respectively. The electronic structure for both defect types of the Eu-doped $La_2Hf_2O_7$ system looks very much similar to that of the undoped system. However, Eu(p) and Eu(d) orbitals contribute to both the VBM and CBM, leading to very small changes in the energy levels of the band edges with respect to that of ideal $La_2Hf_2O_7$ while the Eu(d) states spread throughout the VB and CB.

4.2. Electronic structure of LHOU

To investigate the effect of U doping on the electronic structure of $La_2Hf_2O_7$, we have calculated the DOS for both types of U defects. Fig. 9a shows the DOS plot for U-doped $La_2Hf_2O_7$ with U at the La site (U_{La}) while Fig. 9b shows the DOS plot for U-doped $La_2Hf_2O_7$ with U at the Hf site (U_{Hf}). As can be seen from Fig. 9a, when U substitutes the La site, it introduces shallow defect states just below the CBM by an energy level of 0.55 eV. The defects states are found to be partially occupied in nature. This may be due to the presence of excess electrons in the system. Analysis of PDOS shows that the shallow defect states are mainly composed of U(f) orbitals with minor contribution by U(d) and O(p) orbitals. In contrast, U doping at the Hf lattice site introduces fully occupied impurity states close to the CBM (0.56 eV) (Fig. 9b). These states are contributed mainly by U(f) orbitals with minor contribution by La(d), La (f), and O(p) orbitals.

4.3. Electronic structure of (Eu,U) co-doped $La_2Hf_2O_7$

To investigate the effect of co-doping with U into Eu-doped $La_2Hf_2O_7$, we have calculated the DOS for the four different configurations, *i.e.*, (Eu_{La} + U_{La}), (Eu_{Hf} + U_{Hf}), (Eu_{La} + U_{Hf}), and (U_{La} + La_{Hf}) (Fig. 10). The DOS plot for $La_2Hf_2O_7$ in the presence of Eu and U at the La lattice site as Eu_{La} + U_{La} defects indicates that there exist partially occupied shallow impurity states at 0.70 eV below the CBM (Fig. 10a). The impurity states

3838 | *Inorg. Chem. Front.*, 2021, **8**, 3830–3842

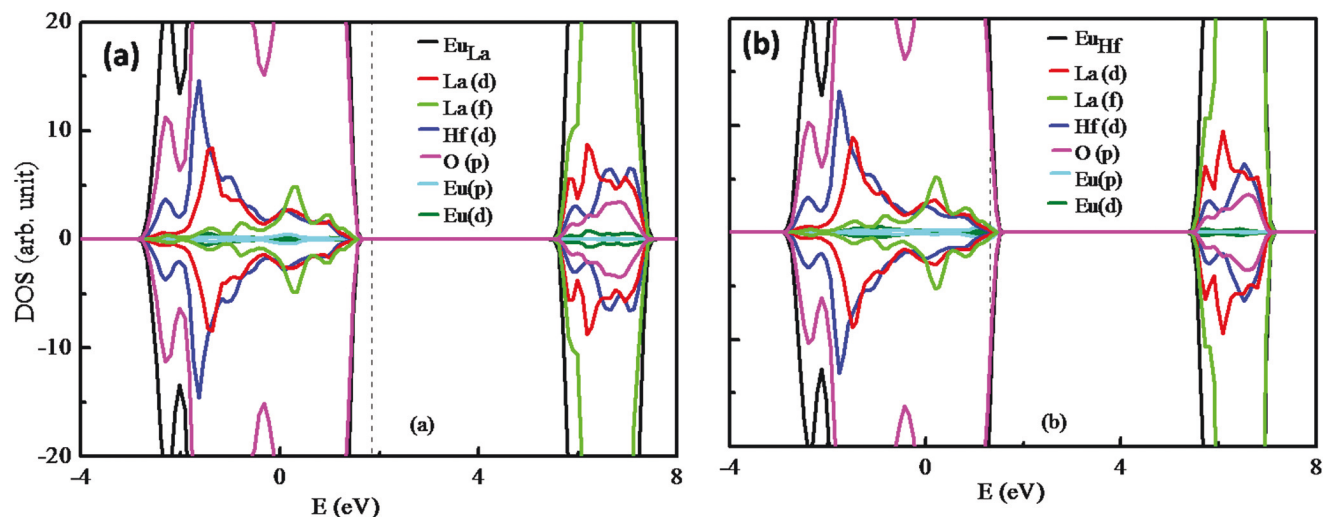This journal is © the Partner Organisations 2021

Fig. 8 Density of states of the (a) Eu_{La} and (b) Eu_{Hf} defects in the LHO host. Vertical dashed line indicates the Fermi level.
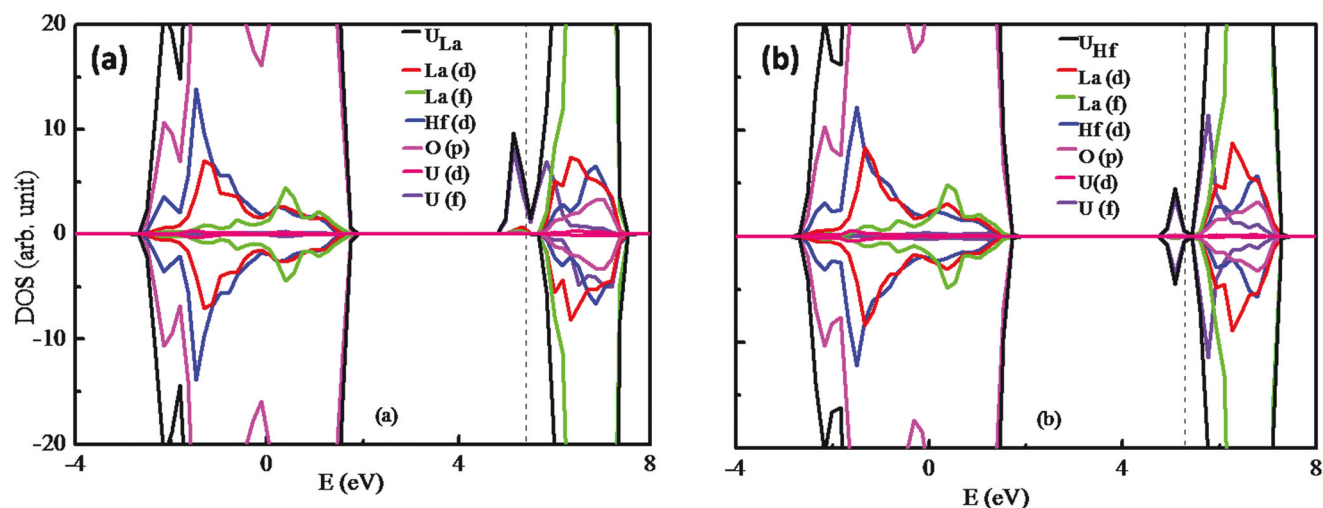

Fig. 9 Density of states of (a) U_{La} and (b) U_{Hf} defects in the LHO host. Vertical dashed line indicates the Fermi level.

are composed of U(f) orbitals. The VBM and CBM levels are found to be lifted by 0.25 eV and 0.19 eV, respectively. The Fermi level is shifted towards the CBM because of excess electrons in the system. The DOS plot for $La_2Hf_2O_7$ in the presence of Eu and U at the Hf lattice sites as $Eu_{Hf} + U_{Hf}$ defects shows that there is a partially occupied impurity state (spin-down direction) at 1.7 eV below the CBM (Fig. 10b). The partially unoccupied impurity states are observed in the forbidden region at 0.21 eV and 0.63 eV below the CBM. The impurity states are mainly composed of U(f) orbitals. The VBM and CBM levels are shifted by 0.18 eV (upward) and 0.14 eV (downward), respectively. Fig. 10c shows the DOS plot for $La_2Hf_2O_7$ in the presence of Eu and U at the La and Hf lattice sites as $Eu_{La} + U_{Hf}$ defects, respectively. In this case, the discrete occupied impurity states are observed at 0.58 eV below the CBM. The occupied impurity states are mainly composed of the U(f) orbital with minor contribution by the O(p) and La(d) orbitals.

The VBM and CBM are increased by 0.15 eV and 0.09 eV with respect to defect free $La_2Hf_2O_7$, respectively. Fig. 10d shows the DOS plot for $La_2Hf_2O_7$ in the presence of Eu and U at the Hf and La lattice sites as $U_{La} + La_{Hf}$ defects, respectively. In this case, partially occupied and unoccupied impurity states are observed at 1.18 eV and 0.57 eV below the CBM, respectively. The occupied impurity states are mainly composed of the U(f) orbital with minor contribution by the O(p) and La(f) orbitals. The VBM is shifted by 0.31 eV (upward) and the CBM is shifted by 0.3 eV (downward) with respect to defect free $La_2Hf_2O_7$, respectively.

Previous studies indicated that monodoping with Eu is accompanied by oxygen vacancy defects, which creates discrete mid-gap states resulting in a significant change in the emission behavior of $La_2Hf_2O_7$ facilitated by the host to europium energy transfer.[9] However, co-doping U into Eu-doped $La_2Hf_2O_7$ makes the system electron rich. Thus, formation of a
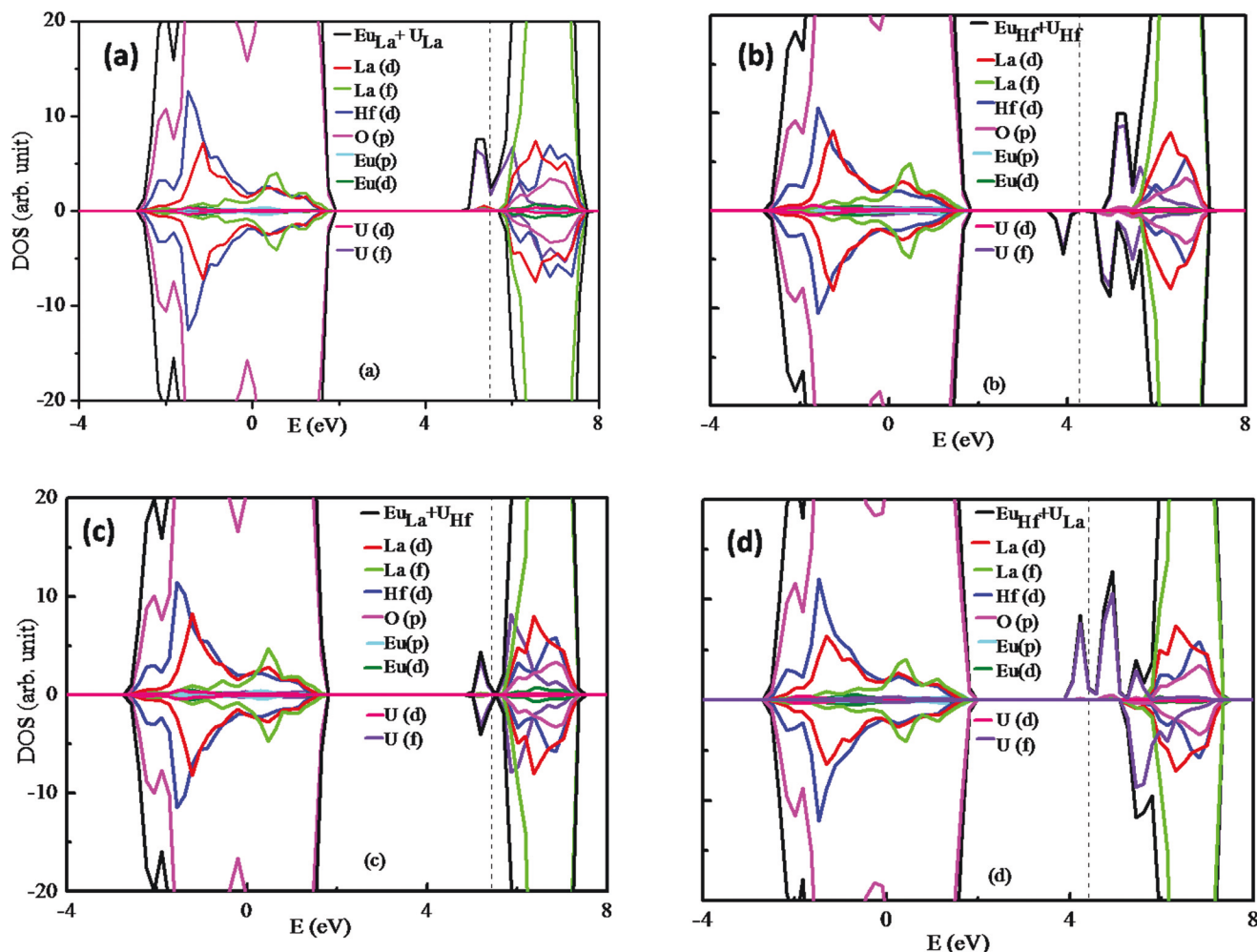
This journal is © the Partner Organisations 2021

Inorg. Chem. Front., 2021, **8**, 3830–3842 | **3839**

Fig. 10 Density of states of (a) $Eu_{La} + U_{La}$, (b) $Eu_{Hf} + U_{Hf}$, (c) $Eu_{La} + U_{Hf}$, and (d) $U_{La} + La_{Hf}$ defects in the LHO host. Vertical dashed line indicates the Fermi level.

cation vacancy is expected to compensate the excess charge in the co-doped system. This indirectly indicates that the formation of an oxygen vacancy is suppressed due to co-doping U into Eu-doped $La_2Hf_2O_7$. In general, the effect of anion vacancy defects is much more prominent on the optical properties than that of the cation vacancy. This is one of factors influencing the change in the optical behavior observed for our Eu-doped $La_2Hf_2O_7$ NPs due to co-doping with U resulting in the inhibition of the host to europium energy transfer.

5. Conclusions

In summary, we synthesized $La_2Hf_2O_7$, $La_2Hf_2O_7:Eu^{3+}$, $La_2Hf_2O_7:U^{6+}$, and $La_2Hf_2O_7:Eu^{3+},U^{6+}$ NPs using a molten salt synthesis method in this work. All these NPs stabilized in an ideal pyrochlore structure with ellipsoidal morphology though uranium co-doping led to enhanced HfO_6 distortion. The undoped LHO NPs displayed defect induced violet-blue emission which can be tuned to red and green emission by doping

europium and uranium, respectively. Here, for the first time, we adopted a novel design strategy to utilize the emission coming from the host, dopant and co-dopant by restricting the host to dopant energy transfer as demonstrated by uranium co-doping into the $La_2Hf_2O_7:Eu^{3+}$ NPs which completely suppressed the HDET by acting as a barrier to enhance the separation between the defect and europium ion. Furthermore, it was found that with increased uranium concentration, the intensity of host emission increased which was triggered by absorption of host emission by the lanthanum and hafnium vacancies and back transfer to the host. Based on DFT calculations, it was found that europium stabilized at the La^{3+} site whereas uranium prefers the Hf^{4+} site making the co-doped system highly electron rich owing to the formation of negatively charged lanthanum and hafnium vacancies. Formation of cation vacancy is expected to compensate the excess charge in the co-doped system while suppressing the formation of oxygen vacancy due to co-doping of U into the Eu-doped $La_2Hf_2O_7$ NPs. Furthermore, the color of emission can also be tuned from blue to green to red by moving from undoped LHO

NPs, to europium doped LHO NPs, and to uranium and europium co-doped LHO NPs. Interestingly, white light emission was observed by co-doping Eu^{3+} (1.0mol%) and U^{6+} (1.0mol%) in the LHOEU NPs.

Conflicts of interest

There are no conflict to declare.

Acknowledgements

References

1 Y. N. Ahn, K. D. Kim, G. Anoop, G. S. Kim and J. S. Yoo, Design of highly efficient phosphor-converted white light-emitting diodes with color rendering indices $(R_1 - R_{15}) \geq 95$ for artificial lighting, *Sci. Rep.*, 2019, **9**, 1–10.

2 J.-S. Li, Y. Tang, Z.-T. Li, J.-X. Li, X.-R. Ding, B.-H. Yu, S.-D. Yu, J.-Z. Ou and H.-C. Kuo, Toward 200 Lumens per Watt of Quantum-Dot White-Light-Emitting Diodes by Reducing Reabsorption Loss, *ACS Nano*, 2021, **15**, 550–562.

3 S. K. Gupta, J. P. Zuniga, M. Abdou, M. P. Thomas, M. D. A. Goonatilleke, B. S. Guiton and Y. Mao, Lanthanide-doped lanthanum hafnate nanoparticles as multicolor phosphors for warm white lighting and scintillators, *Chem. Eng. J.*, 2020, **379**, 122314.

4 S. K. Gupta, V. Grover, R. Shukla, K. Srinivasu, V. Natarajan and A. K. Tyagi, Exploring pure and RE co-doped (Eu^{3+}, Tb^{3+} and Dy^{3+}) gadolinium scandate: Luminescence behaviour and dynamics of energy transfer, *Chem. Eng. J.*, 2016, **283**, 114–126.

5 M. Abdou, S. K. Gupta, J. P. Zuniga and Y. Mao, On structure and phase transformation of uranium doped $La_2Hf_2O_7$ nanoparticles as an efficient nuclear waste host, *Mater. Chem. Front.*, 2018, **2**, 2201–2211.

6 S. K. Gupta, M. Abdou, P. S. Ghosh, J. P. Zuniga, E. Manoharan, H. Kim and Y. Mao, On comparison of luminescence properties of $La_2Zr_2O_7$ and $La_2Hf_2O_7$ nanoparticles, *J. Am. Ceram. Soc.*, 2020, **103**, 235–248.

7 S. K. Gupta, M. Abdou, J. P. Zuniga, A. A. Puretzky and Y. Mao, Samarium-Activated $La_2Hf_2O_7$ Nanoparticles as Multifunctional Phosphors, *ACS Omega*, 2019, **4**, 17956–17966.

8 S. K. Gupta, J. P. Zuniga, M. Abdou and Y. Mao, Thermal annealing effects on $La_2Hf_2O_7$:Eu^{3+} nanoparticles: a curious case study of structural evolution and site-specific photo- and radio-luminescence, *Inorg. Chem. Front.*, 2018, **5**, 2508–2521.

9 S. K. Gupta, J. P. Zuniga, P. S. Ghosh, M. Abdou and Y. Mao, Correlating Structure and Luminescence Properties of Undoped and Eu^{3+}-Doped $La_2Hf_2O_7$ Nanoparticles Prepared with Different Coprecipitating pH Values through Experimental and Theoretical Studies, *Inorg. Chem.*, 2018, **57**, 11815–11830.

10 Y. Ji, D. Jiang and J. Shi, $La_2Hf_2O_7$:Ti^{4+} ceramic scintillator for X-ray imaging, *J. Mater. Res.*, 2005, **20**, 567–570.

11 Y. M. Ji, D. Y. Jiang, Y. K. Liao and J. L. Shi, Fabrication and Spectroscopic Investigation of $La_2Hf_2O_7$-Based Phosphors, *Key Eng. Mater.*, 2004, **280–283**, 577–580.

12 Y.-m. Ji, D.-y. Jiang and J.-l. Shi, Preparation and spectroscopic properties of $La_2Hf_2O_7$/Tb, *Mater. Lett.*, 2005, **59**, 868–871.

13 J. Trojan-Piegza, S. Gierlotka, E. Zych and W. Lojkowski, Spectroscopic Studies of Nanopowder and Nanoceramics $La_2Hf_2O_7$:Pr Scintillator, *J. Am. Ceram. Soc.*, 2014, **97**, 1595–1601.

14 J. Trojan-Piegza and E. Zych, White persistent luminescence of $La_2Hf_2O_7$:Ti,Pr, *Opt. Mater.*, 2021, **113**, 110896.

15 J. Trojan-Piegza, E. Zych and M. Kosińska, Fabrication and spectroscopic properties of nanocrystalline $La_2Hf_2O_7$:Pr, *Radiat. Meas.*, 2010, **45**, 432–434.

16 J. Zhang, K. Tse, M. Wong, Y. Zhang and J. Zhu, A brief review of co-doping, *Front. Phys.*, 2016, **11**, 117405.

17 W. Luo, R. Li and X. Chen, Host-Sensitized Luminescence of Nd^{3+} and Sm^{3+} Ions Incorporated in Anatase Titania Nanocrystals, *J. Phys. Chem. C*, 2009, **113**, 8772–8777.

18 S. K. Gupta, R. Kadam and P. Pujari, Lanthanide spectroscopy in probing structure-property correlation in multi-site photoluminescent phosphors, *Coord. Chem. Rev.*, 2020, **420**, 213405.

19 A. Biswas, R. Bakthavatsalam and J. Kundu, Efficient Exciton to Dopant Energy Transfer in Mn^{2+}-Doped $(C_4H_9NH_3)_2PbBr_4$ Two-Dimensional (2D) Layered Perovskites, *Chem. Mater.*, 2017, **29**, 7816–7825.

20 J. Llanos, D. Espinoza and R. Castillo, Energy transfer in single phase Eu^{3+}-doped Y_2WO_6 phosphors, *RSC Adv.*, 2017, **7**, 14974–14980.

21 Z. Xianju, Y. Xiaodong, X. Tengjiao, Z. Kaining, C. Tianyu, Y. Hao and W. Zhongqing, Luminescence properties and energy transfer of host sensitized $CaMoO_4$:Tb^{3+} green phosphors, *J. Rare Earths*, 2013, **31**, 655–659.

22 S. K. Gupta, P. S. Ghosh, N. Pathak, A. Arya and V. Natarajan, Understanding the local environment of Sm^{3+} in doped $SrZrO_3$ and energy transfer mechanism using time-resolved luminescence: a combined theoretical and experimental approach, *RSC Adv.*, 2014, **4**, 29202–29215.

23 S. K. Gupta, P. S. Ghosh, A. K. Yadav, S. N. Jha, D. Bhattacharyya and R. M. Kadam, Origin of Blue-Green Emission in α-$Zn_2P_2O_7$ and Local Structure of Ln^{3+} Ion in α-$Zn_2P_2O_7$:Ln^{3+} (Ln = Sm, Eu): Time-Resolved Photoluminescence, EXAFS, and DFT Measurements, *Inorg. Chem.*, 2017, **56**, 167–178.

This journal is © the Partner Organisations 2021

Inorg. Chem. Front., 2021, **8**, 3830–3842 | **3841**

24 S. K. Gupta, P. S. Ghosh, A. K. Yadav, N. Pathak, A. Arya, S. N. Jha, D. Bhattacharyya and R. M. Kadam, Luminescence Properties of SrZrO₃/Tb³⁺ Perovskite: Host-Dopant Energy-Transfer Dynamics and Local Structure of Tb³⁺, *Inorg. Chem.*, 2016, **55**, 1728–1740.

25 S. K. Gupta, M. Sahu, P. S. Ghosh, D. Tyagi, M. K. Saxena and R. M. Kadam, Energy transfer dynamics and luminescence properties of Eu³⁺ in CaMoO₄ and SrMoO₄, *Dalton Trans.*, 2015, **44**, 18957–18969.

26 N. S. Singh, N. K. Sahu and D. Bahadur, Multicolor tuning and white light emission from lanthanide doped YPVO₄ nanorods: energy transfer studies, *J. Mater. Chem. C*, 2014, **2**, 548–555.

27 W. Lee, J. W. Han, Y. Chen, Z. Cai and B. Yildiz, Cation Size Mismatch and Charge Interactions Drive Dopant Segregation at the Surfaces of Manganite Perovskites, *J. Am. Chem. Soc.*, 2013, **135**, 7909–7925.

28 L. Lv, T. Wang, S. Li, Y. Su and X. Wang, Tuning the optical, electronic and luminescence properties of LaOCl: Eu³⁺ via structural and lattice strain modulation, *CrystEngComm*, 2016, **18**, 907–916.

29 W. J. Chung and J. Y. Lee, The role of the bulky blocking unit of the fluorescent emitter in efficient green hyper-fluorescent organic light-emitting diodes, *J. Inf. Disp.*, 2020, 1–6.

30 F. Kang, L. Li, J. Han, D. Y. Lei and M. Peng, Emission color tuning through manipulating the energy transfer from VO4³⁻ to Eu³⁺ in single-phased LuVO₄:Eu³⁺ phosphors, *J. Mater. Chem. C*, 2017, **5**, 390–398.

31 M. Kumar and M. Mohapatra, A case study of energy transfer mechanism from uranium to europium in ZnAl₂O₄ spinel host by photoluminescence spectroscopy, *Spectrochim. Acta, Part A*, 2016, **159**, 42–47.

32 P. E. Blöchl, Projector augmented-wave method, *Phys. Rev. B: Condens. Matter Mater. Phys.*, 1994, **50**, 17953.

33 G. Kresse and D. Joubert, From ultrasoft pseudopotentials to the projector augmented-wave method, *Phys. Rev. B: Condens. Matter Mater. Phys.*, 1999, **59**, 1758.

34 J. P. Perdew, K. Burke and M. Ernzerhof, Generalized gradient approximation made simple, *Phys. Rev. Lett.*, 1996, **77**, 3865.

35 J. P. Perdew, J. A. Chevary, S. H. Vosko, K. A. Jackson, M. R. Pederson, D. J. Singh and C. Fiolhais, Atoms, molecules, solids, and surfaces: Applications of the generalized gradient approximation for exchange and correlation, *Phys. Rev. B: Condens. Matter Mater. Phys.*, 1992, **46**, 6671.

36 H. J. Monkhorst and J. D. Pack, Special points for Brillouin-zone integrations, *Phys. Rev. B: Solid State*, 1976, **13**, 5188.

37 M. Subramanian, G. Aravamudan and G. S. Rao, Oxide pyrochlores—a review, *Prog. Solid State Chem.*, 1983, **15**, 55–143.

38 F. N. Sayed, V. Grover, K. Bhattacharyya, D. Jain, A. Arya, C. Pillai and A. Tyagi, Sm₂₋ₓDyₓZr₂O₇ pyrochlores: probing order– disorder dynamics and multifunctionality, *Inorg. Chem.*, 2011, **50**, 2354–2365.

39 K. M. Turner, D. R. Rittman, R. A. Heymach, C. L. Tracy, M. L. Turner, A. F. Fuentes, W. L. Mao and R. C. Ewing, Pressure-induced structural modifications of rare-earth hafnate pyrochlore, *J. Phys.: Condens. Matter*, 2017, **29**, 255401.

40 J. P. Zuniga, S. K. Gupta, M. Abdou and Y. Mao, Effect of molten salt synthesis processing duration on the photo- and radioluminescence of UV-, Visible-, and X-ray-excitable La₂Hf₂O₇:Eu³⁺ nanoparticles, *ACS Omega*, 2018, **3**, 7757–7770.

41 M. Pokhrel, S. K. Gupta, K. Wahid and Y. Mao, Pyrochlore Rare-Earth Hafnate RE₂Hf₂O₇ (RE = La and Pr) Nanoparticles Stabilized by Molten-Salt Synthesis at Low Temperature, *Inorg. Chem.*, 2019, **58**, 1241–1251.

42 N. Garg, K. K. Pandey, C. Murli, K. V. Shanavas, B. P. Mandal, A. K. Tyagi and S. M. Sharma, Decomposition of lanthanum hafnate at high pressures, *Phys. Rev. B: Condens. Matter Mater. Phys.*, 2008, **77**, 214105.

43 A. Slifka, B. Filla, J. Phelps, G. Bancke and C. Berndt, Thermal conductivity of a zirconia thermal barrier coating, *J. Therm. Spray Technol.*, 1998, **7**, 43–46.

44 H. Yamamura, H. Nishino, K. Kakinuma and K. Nomura, Electrical conductivity anomaly around fluorite–pyrochlore phase boundary, *Solid State Ionics*, 2003, **158**, 359–365.

45 P. Modak and B. Modak, Insight into enhanced thermoluminescence property of (Mg, Cu, Ag)-Doped LiF: A DFT study, *J. Lumin.*, 2021, **231**, 117779.

46 P. Modak and B. Modak, Exploring the role of vacancy defects in the optical properties of LiMgPO₄, *Phys. Chem. Chem. Phys.*, 2020, **22**, 16244–16257.

47 S. K. Gupta, K. Sudarshan, P. S. Ghosh, A. P. Srivastava, S. Bevara, P. K. Pujari and R. M. Kadam, Role of various defects in the photoluminescence characteristics of nanocrystalline Nd₂Zr₂O₇: an investigation through spectroscopic and DFT calculations, *J. Mater. Chem. C*, 2016, **4**, 4988–5000.

48 X. Qin, X. Liu, W. Huang, M. Bettinelli and X. Liu, Lanthanide-Activated Phosphors Based on 4f-5d Optical Transitions: Theoretical and Experimental Aspects, *Chem. Rev.*, 2017, **117**, 4488–4527.

49 D. L. Dexter, A Theory of Sensitized Luminescence in Solids, *J. Chem. Phys.*, 1953, **21**, 836–850.

50 S. A. Vieira, N. Rakov, C. B. de Araújo and E. L. Falcão-Filho, Upconversion luminescence in europium doped Y₂O₃ powder excited by absorption of three, four, and five infrared photons, *Opt. Mater. Express*, 2019, **9**, 3952–3961.

3842 | *Inorg. Chem. Front.*, 2021, **8**, 3830–3842

This journal is © the Partner Organisations 2021